IMPACT OF HARBOR NAVIGATION CHANNELS ON WAVES: A NUMERICAL MODELLING GUIDELINE

D.W. Dusseljee[1], G. Klopman[2], G. Ph. van Vledder[3] and H.J. Riezebos[4]

This study presents an intercomparison of a SWAN and SWASH wave model and 3D laboratory experiments for an existing navigation channel towards a harbor. Results show that the spectral refraction model SWAN underestimates the wave conditions in the channel and at the lee side of the channel especially - for longer waves travelling under a small angle with the channel - due to the neglect of the effects of wave tunneling by diffraction and evanescent modes. The phase-resolving non-hydrostatic 3D model SWASH does include these effects and performs reasonably well, though computational CPU demands are much higher. A modelling guideline is presented for application to other situations, showing that these effects need to be taken into account in optimizing the (layout) of the harbor; otherwise it may lead to under- or overestimation of the wave conditions and wave penetration into a harbor basin.

Keywords: Wave modelling, navigation channels, laboratory experiments, SWAN, SWASH.

INTRODUCTION

Numerical modelling of a navigation channel

The presence of a navigation channel modifies the wave conditions, both outside and inside a harbor. This requires that the – often long – navigation channel is taken into account in the determination of the relevant wave conditions in the harbor and the surrounding nearshore area. In case of waves encountering a navigation channel in intermediate and shallow water depths, there may be conditions under which part of the waves do not cross the channel, but are reflected by refraction (Zwamborn and Grieve, 1974). Numerical models as well as physical models may be used to assess the impact of the navigation channel on the wave conditions (Misra et al., 2008; Guzman Mardones, 2011; Dusseljee et al., 2012). Different types of models have their own capabilities and limitations, and it is important to know in advance whether a certain modelling strategy will provide accurate enough answers for the analyzed harbor and navigation channel layout.

For a first assessment of the wave conditions outside the harbor, given metocean conditions and bathymetry, nowadays often a phase-averaged spectral wave-energy model is used. These models are relatively easy in their set-up and fast with computational results. Several of these programs have been extensively validated, using data from field and laboratory measurements. For many situations, the refraction modelling in combination with multidirectional incoming random waves is adequate for providing accurate predictions of the wave conditions outside the harbor.

When diffraction effects are important, e.g. within the harbor or behind (barrier) islands, phase-resolving numerical models are most often required. Although, in spectral wave-energy models, some diffraction effects can be taken into account – by the method of Holthuijsen et al. (2003). The phase-resolving models require much finer grids than the spectral wave-energy models: the spatial grid size has to be small compared to the wavelength (while in the spectral wave-energy models the changes in bathymetry primarily dictate the required spatial resolution). As a result, phase-resolving numerical models require much larger computer resources (in both memory and CPU-time demands) than phase-averaged energy-spectra models. Consequently, these models are most often only applicable for computing the wave agitation in harbor basins (and eventually a relatively small region outside the harbor). Many types of phase-resolving models exist. Classically, the mild-slope equation (Berkhoff, 1973; Booij, 1983, Hurdle et al., 1989) and Boussinesq-type wave models (Kirby, 2003; Ma, 2010) have been used. Nowadays, also three-dimensional non-hydrostatic wave models are applied more-and-more (e.g. Zijlema et al. , 2011; Van Vledder and Zijlema, 2014).

Physical modelling of a navigation channel

Physical laboratory tests are most demanding in resources. They usually require quite some time to set-up, perform and analyze. On the one hand, measurements are often restricted to a number of points at which measuring gauges are deployed. On the other hand, before-mentioned numerical modelling techniques provide additional insight by providing information in the whole computational domain. The advantage of physical model tests is, that if set up properly, they include all (or most) physical effects – also of processes which are difficult (or impossible) to compute. Due to conflicting scale laws

[1] Witteveen+Bos Consulting Engineers, P.O. Box 233, Deventer, 7400 AE, The Netherlands
[2] Witteveen+Bos Consulting Engineers, P.O. Box 233, Deventer, 7400 AE, The Netherlands
[3] Delft University of Technology, P.O. Box 2048, Delft, 2600 GA, The Netherlands, now at Van Vledder Consulting
[4] Deltares, P.O. Box 177, Delft, 2600 MH, The Netherlands

(e.g. Froude and Reynolds), instrument resolution and inaccuracy, and limited available laboratory space, the area covered by a physical model test is relatively small. Often only the harbor itself and a small region in front of it can be modeled.

Purpose

Here, we will present results on wave transformation by a navigation channel, derived from three types of multi-directional random-wave models: a spectral refraction model (SWAN; Booij et al. 1999), a phase-resolving non-hydrostatic 3D model (SWASH; Zijlema et al., 2011) and physical model laboratory tests (Dusseljee et al., 2012); in order to determine an effective modelling approach for engineering purposes. The intercomparison is performed by setting up numerical SWAN and SWASH models of the laboratory experiment, which represents an existing navigation channel towards a harbor, for a number of scenarios. The relevant wave parameters and wave spectra are compared for random incident multi-directional waves.

WAVE PROCESSES INVOLVED

Wave refraction

According to refraction theory there are (trans)critical conditions under which incident periodic waves cannot cross a straight channel: waves – not in deep water conditions and travelling in a direction closer than a critical angle θ_{cr} to the channel axis – are reflected on the downward channel slope by refraction. Waves travelling in a direction more perpendicular to the channel axis than a critical angle $\theta < \theta_{cr}$ may cross the channel. The angle θ is defined as the angle between the incident wave crests and the channel axis, *i.e.* $\theta = 0°$ corresponds with waves propagating perpendicularly to the channel axis and $\theta = 90°$ corresponds with waves propagating parallel to the channel axis. The critical angle θ_{cr} between the wave propagation direction and the direction normal to the channel axis depends on the phase speeds of the wave components outside the channel (c_1) and in the deepest part of the channel (c_2): $\theta_{cr} = \arccos(c_1 / c_2)$. The occurrence of wave reflection above the critical angle was confirmed by experiment (e.g. Zwamborn and Grieve, 1974). In the approximation using refraction theory, the capacity of waves to cross a channel (transmission) only depends on the water depth inside and outside the channel, see Fig. 1. It does not depend on the width or cross-sectional shape of the channel.

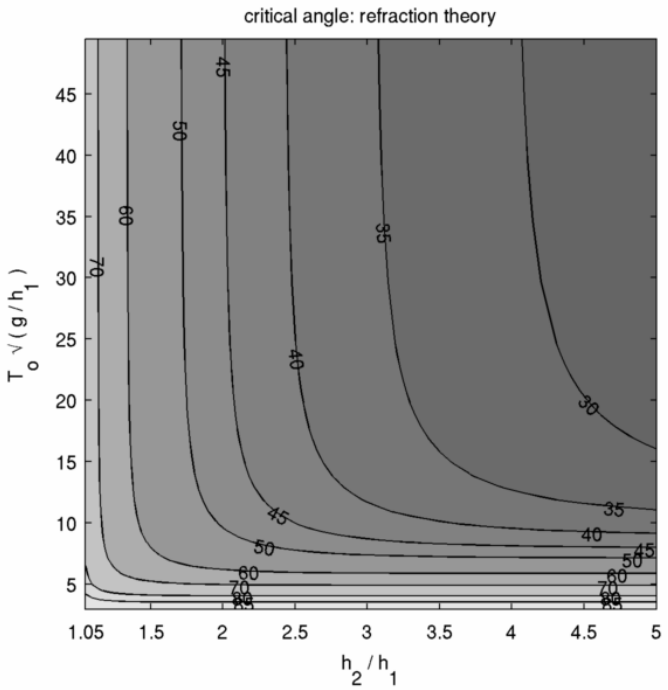

Figure 1. Critical wave angle θ_{cr} based on refraction theory as a function of dimensionless wave period outside the channel $T_0\sqrt{(g/h_1)}$ and the water depth ratio h_2/h_1 outside and inside the navigation channel.

Wave diffraction and nonlinear effects

When diffraction effects are taken into account, the width and cross-sectional shape of the channel also affect the reflection and transmission of waves. Waves may partially be transmitted across the channel even though the incident wave direction is above the critical angle (Kirby & Dalrymple, 1983, Li et al., 2000). Due to the combined effect of refraction, reflection and diffraction, wave components propagating along the channel and decaying exponentially (evanescent) in the cross-channel direction – analogous to edge waves – occur, see Fig. 2(a), also in transcritical conditions $\theta > \theta_{cr}$. This allows for part of the wave energy to be transmitted to the leeward side of the channel. This effect is called tunneling, in analogy with the similar effect in quantum mechanics. Magne et al. (2007) showed that this effect allows waves to cross a deep nearshore canyon.

The simplest models in use, which include both refraction and diffraction, are the so-called mild-slope models (Berkhoff, 1972; Booij, 1983; Porter, 2003). The latter (Porter, 2003) contains a revised mild-slope equation of simple form with improved reflection behavior (for additional reflections induced by the channel slopes).

Higher order effects include those of evanescent modes: additional spatial-decaying modes as induced by the channel slopes and partial wave reflection (Kirby and Dalrymple, 1983). Boussinesq-type wave models include more evanescent modes. Layered non-hydrostatic models can include many evanescent modes, with the number of modes increasing with the number of layers employed. Other effects which may be important are nonlinear wave interactions, bottom friction, wave breaking and whitecapping, wind forcing, wave–current interaction and turbulence effects.

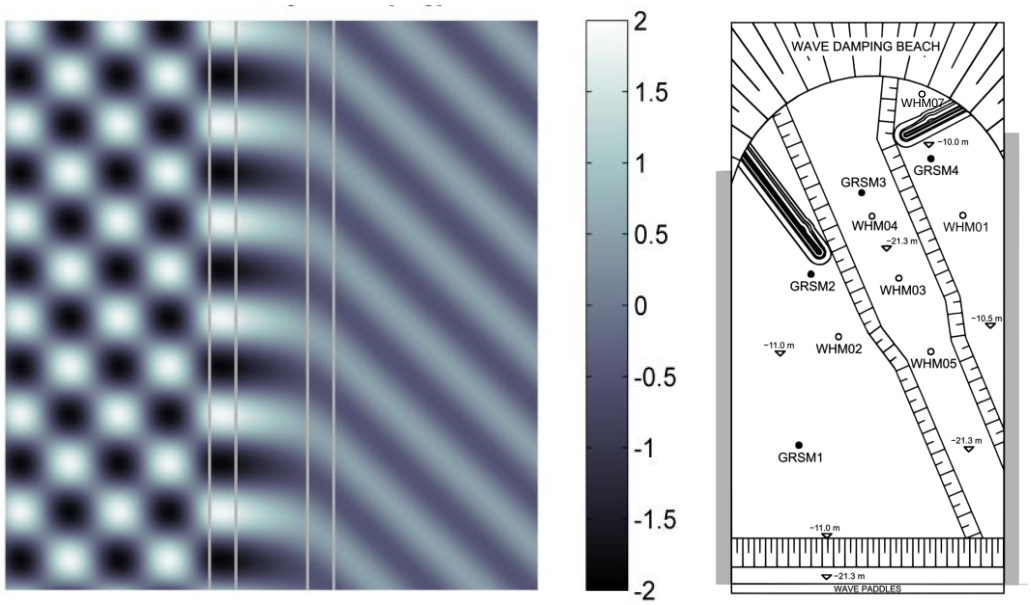

Figure 2. (a) Surface elevation in combined refraction and diffraction of waves incident at the critical angle. On the left the cross-wave pattern of incident (45°) and reflected waves; in the channel exponential-decaying (evanescent) modes; on the right transmitted waves; (b) model setup for the navigation channel towards the harbor.

PHYSICAL AND NUMERICAL MODEL SETUP

Physical model setup

The experiment represents an existing navigation channel towards a harbor, with a long straight access channel of length 15 km; see Fig. 2(b) for the experimental set-up of the harbor entrance. Waves are generated at deep water (water depth of -21.3 m), which is also the water depth in the access channel. A gentle transition slope (1:10) guides the waves to the actual foreshore of the harbor with a water depth of 12.5 m. The side slopes of the access channel are designed with a 1:5 slope. The width of the channel at the bottom is 250 m near the harbor entrance (between the two breakwaters) and 170 m further offshore.

The physical scale-model tests are performed in a 3D wave basin of Deltares in The Netherlands, which is equipped with a multi-directional wave generator, able to generate short-crested random waves. The wave generators are equipped with active wave absorption to prevent reflected waves (generated by structures and bathymetry in the basin) to re-reflect on the wave paddles. Second-order wave maker steering of random Stokes waves is applied – for the generation of realistic sharp-crested shapes of the individual waves as well as wave-group-bound long waves. This second-order control prevents to a large extend the generation of spurious sub- and super-harmonic free waves.

The physical model is Froude scaled at scale 1:60, implying that most wave processes are correctly included, as compared with prototype conditions. Bed friction will be overestimated in the scale model, since bed friction has a Reynolds scaling, but is of minor importance due to the small distance – in number of wave lengths, of the order ten – over which the waves travel.

The applied orientation of the incident waves is 0° (normal to the wave paddles) for all tests. The waves approach the access channel with an incident angle of 23°. At the basin end a wave damping beach is installed to dissipate all wave energy. A normal distributed directional spreading (with 20° standard deviation; as defined by Kuik et al. (1988)) is applied.

Wave conditions are measured at several locations, as indicated in Fig. 2(b). The open circles are standard resistant type wave gauges (WHM). The closed circles are directional wave gauges (GRSM).

Numerical model setup

A numerical SWAN and SWASH model of the physical experiment are set up. In both models, the navigation channel is modelled on a uniform rectilinear grid, using a 3x3m grid size. The resulting number of cells per deep water wave length (L_0) is slightly below 50. For SWASH, this rather low value is used to reduce CPU-time demands, while keeping a minimal level of accuracy. The exact bathymetry as used in the physical model is implemented in the numerical models. The breakwaters are implemented as porous structures and as partially reflecting line obstacles in SWASH and SWAN respectively, calculating the wave transmission per wave frequency. In SWASH, a porosity of 0.45 is applied. In SWAN, transmission is computed based on d'Angremond et al. (1996).

In SWAN, (nonlinear) wave processes like wave breaking, nonlinear wave interactions, whitecapping, bottom friction and wave growth by wind input are included. Although SWAN may provide approximations to diffraction effects, these have not been used: SWAN's requirement that diffracting features are large compared to the wave length is not met. In our case the channel width is only a few wave lengths (under extreme conditions). Inclusion of approximate diffraction may lead to underestimating the near-channel wave height along the wave-ward breakwater (Dusseljee et al., 2012).

In SWASH, the wave damping beach at the end of the physical model is replaced by a wave-dissipating sponge layer. In the vertical, 2 terrain following layers are employed. The application of two layers should be sufficient, as it theoretically allows for accurate modelling of waves with periods of 4s or more; the restriction due to the grid resolution is more stringent: adding more vertical layers does not improve the accuracy.

Test conditions

Two distinguished wave scenarios are presented, with relatively small wave angles between the incident wave direction and channel axis. A single peaked wind-sea wave spectrum (case C1) and a double peaked spectrum including both local wind conditions and swell (case C2) are applied. Table 1 summarizes the imposed conditions at the target location outside the area of channel influence (GRSM1). In both the numerical and the physical models, the wave boundaries are applied as 2D wave spectra, with a directional wave spreading of 20°.

Table 1. Imposed incident wave conditions at target location (GRSM1).

Scenario	H_{m0} (m)	T_p (s)	$T_{m-1,0}$ (s)
C1	3.0	9.7	7.9
C2	4.8	14.1	10.7

The two-dimensional wave spectrum at the GRSM1 wave gauge for scenario C2, including indication of the critical wave angle by refraction theory for our experimental setup is presented in Fig. 3. It can be observed that it most wave energy is expected to focus along the wave-ward side of the channel for this scenario.

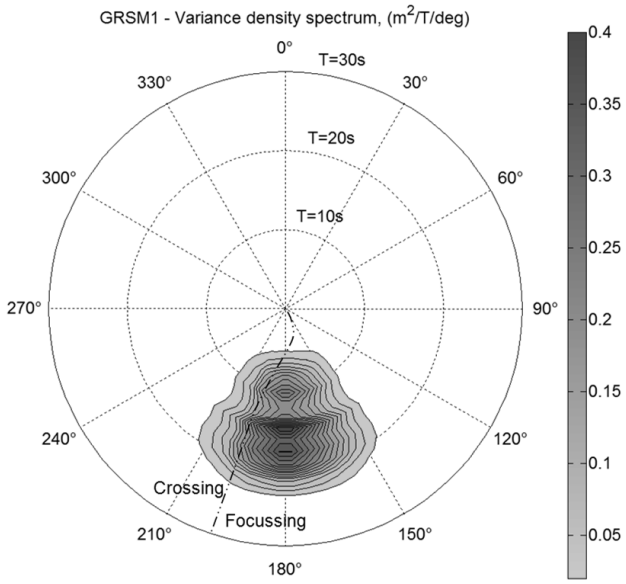

Figure 3. Two-dimensional wave spectrum at the GRSM1 wave gauge, including indication of the critical wave angle θ_{cr}.

RESULTS

Results of the SWAN and SWASH models and the physical model are presented, for both scenarios.

Fig. 4 presents the spatial distributions of the significant wave height H_{m0} by SWAN and SWASH for scenario C1 and C2. In both cases, and scenario C2 in particular (refraction/reflection is wave frequency dependent), a substantial part of the incoming multi-directional wave spectrum travels at angles where waves (theoretically) do not cross the channel. Wave energy concentration occurs along the wave-ward side of the channel and waves break, resulting in a 'sharp edge' of wave energy along the channel, especially for the SWAN results, causing diffraction effects to occur. The significant wave heights, computed by SWAN, at the lee-ward side of the channel are significantly lower than computed by SWASH, possibly due to the neglect of the effects of wave tunneling into and across the channel by diffraction (and to a lesser extent by evanescent modes and non-linear phase speed).

In SWASH, it was found that the high wave frequencies (of 0.13 Hz and higher), significantly dampen over the first few grid cells, due to a relatively low spatial resolution of the SWASH model, resulting in an inaccurate reproduction of the upper part of the spectrum. This can be observed in Fig. 4, as the overall (undisturbed) wave height is lower in SWASH. Sensitivity simulations show that a horizontal grid resolution of 0.5m, combined with a vertical resolution of at least 3 layers would be required to accurately model the full spectrum (up to 0.35 Hz). As such simulations would not be feasible due to computational restraints, we have presented the significant wave height based on the lower part of the spectrum (up to 0.13 Hz) – for both the numerical models and the physical model – separately in Tables 2-5. For both scenarios, the dampened high frequencies in SWASH have a significantly higher critical angle θ_{cr} to the channel axis (Fig. 1) than the lower frequencies and thus these frequencies cross the channel by refraction theory. Therefore, in this study we do not consider these higher frequencies; the different models – and the underlying physical processes – all sufficiently account for refraction.

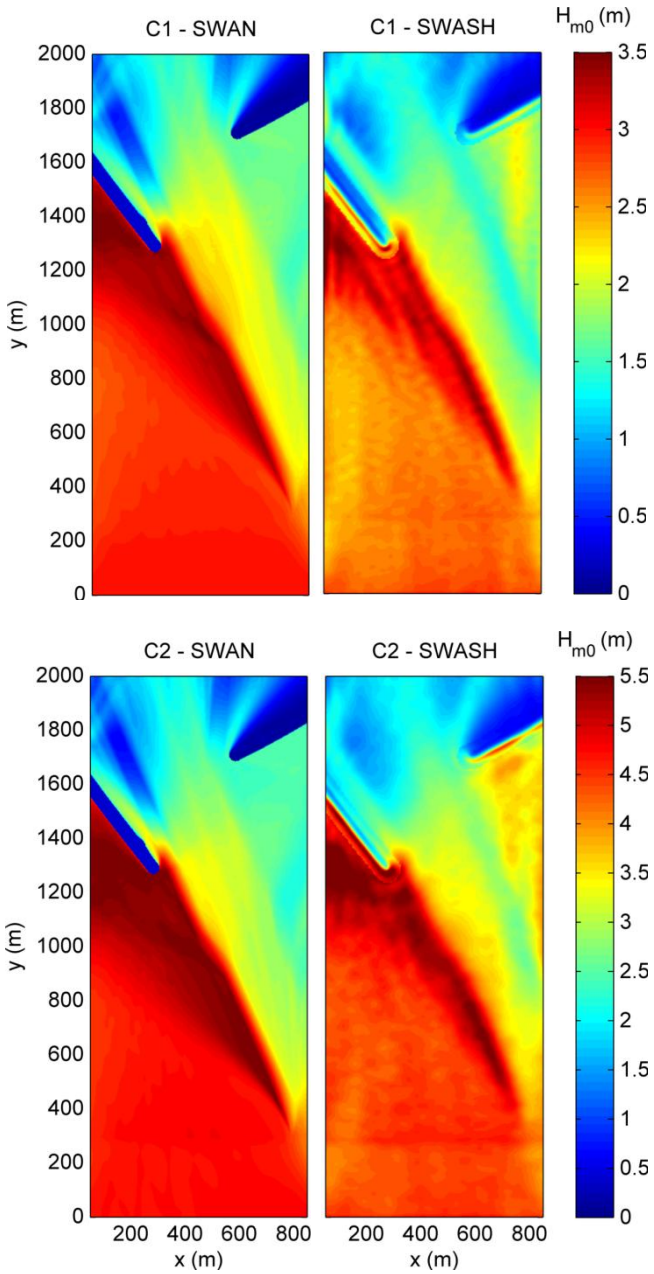

Figure 4. Spatially varying significant wave heights Hm0 (m), as computed by SWAN (left) and SWASH (right). Top: scenario C1. Bottom: scenario C2.

Tables 2-5 present the intercomparison of the modelled wave conditions and the measured conditions in terms of significant wave height and spectral mean and peak wave periods at the wave gauges, see Fig. 2(b) for the wave gauge locations. Figures 5 and 6 present the intercomparison of the modelled and measured wave spectra at the wave gauges, for scenario C1 and C2 respectively.

Table 2. Results C1, significant wave height H_{m0} (m)

	PHM H_{m0} (m)	PHM $H_{m0,<0.13Hz}$ (m)	SWS H_{m0} (m)	SWS $H_{m0,<0.13Hz}$ (m)	SWN H_{m0} (m)	SWN $H_{m0,<0.13Hz}$ (m)
GRSM1	3.03	2.08	2.51 (-17%)	1.93 (-7%)	2.82 (-7%)	1.94 (-7%)
GRSM2	3.63	2.76	3.14 (-13%)	2.64 (-4%)	3.36 (-7%)	2.54 (-8%)
GRSM3	2.36	1.45	1.80 (-24%)	1.37 (-5%)	2.06 (-13%)	1.26 (-13%)
GRSM4	2.50	1.48	1.85 (-26%)	1.38 (-7%)	1.64 (-34%)	0.95 (-36%)
WHM01	2.81	1.85	2.07 (-26%)	1.70 (-8%)	1.60 (-43%)	0.95 (-49%)
WHM02	3.55	2.57	3.25 (-8%)	2.74 (+7%)	3.30 (-7%)	2.49 (-3%)
WHM03	2.77	1.63	1.93 (-30%)	1.43 (-12%)	2.15 (-22%)	1.32 (-19%)
WHM04	2.60	1.52	1.88 (-28%)	1.44 (-5%)	2.11 (-19%)	1.31 (-14%)
WHM05	2.73	1.52	1.85 (-32%)	1.32 (-14%)	2.10 (-23%)	1.22 (-20%)
WHM07	1.30	0.75	0.89 (-32%)	0.73 (-2%)	1.33 (+2%)	0.98 (+31%)

Table 3. Results C1, spectral mean and peak wave periods $T_{m-1,0}$ and T_p (s)

	PHM $T_{m-1,0}$ (s)	PHM T_p (s)	SWS $T_{m-1,0}$ (s)	SWS T_p (s)	SWN $T_{m-1,0}$ (s)	SWN T_p (s)
GRSM1	7.86	9.72	8.60 (+9%)	9.66 (-1%)	7.33 (-7%)	9.70 (-0%)
GRSM2	8.31	9.14	8.91 (+7%)	8.86 (-3%)	7.92 (-5%)	9.70 (+6%)
GRSM3	7.22	9.72	8.32 (+15%)	9.35 (-4%)	6.94 (-4%)	8.83 (-9%)
GRSM4	7.08	10.36	8.61 (+22%)	9.94 (-4%)	6.55 (-7%)	9.70 (-6%)
WHM01	7.64	10.36	8.89 (+16%)	8.90 (-14%)	6.60 (-14%)	9.70 (-6%)
WHM02	8.09	9.72	8.92 (+10%)	9.75 (+0%)	7.89 (-2%)	9.70 (-0%)
WHM03	7.18	9.14	8.32 (+16%)	9.06 (-1%)	6.87 (-4%)	9.70 (+6%)
WHM04	7.10	9.14	8.29 (+17%)	8.82 (-3%)	6.92 (-3%)	9.70 (+6%)
WHM05	6.96	6.76	8.16 (+17%)	9.43 (+40%)	6.63 (-5%)	8.83 (+31%)
WHM07	7.14	9.14	8.91 (+25%)	9.18 (+0%)	7.80 (+9%)	9.70 (+6%)

Table 4. Results C2, significant wave height H_{m0} (m)

	PHM H_{m0} (m)	PHM $H_{m0,<0.13Hz}$ (m)	SWS H_{m0} (m)	SWS $H_{m0,<0.13Hz}$ (m)	SWN H_{m0} (m)	SWN $H_{m0,<0.13Hz}$ (m)
GRSM1	4.80	3.74	4.37 (-9%)	3.56 (-5%)	4.64 (-3%)	3.74 (-0%)
GRSM2	5.33	4.39	5.26 (-1%)	4.46 (+2%)	5.42 (+2%)	4.66 (+6%)
GRSM3	3.56	2.73	2.96 (-17%)	2.49 (-9%)	2.93 (-18%)	2.16 (-21%)
GRSM4	4.31	3.37	3.82 (-11%)	3.21 (-5%)	2.37 (-45%)	1.67 (-50%)
WHM01	4.36	3.31	3.42 (-22%)	2.89 (-13%)	2.42 (-44%)	1.75 (-47%)
WHM02	5.36	4.41	5.26 (-2%)	4.46 (+1%)	5.44 (+2%)	4.66 (+6%)
WHM03	4.42	3.37	3.40 (-23%)	2.94 (-13%)	3.16 (-29%)	2.32 (-31%)
WHM04	3.98	2.98	3.14 (-21%)	2.60 (-13%)	3.07 (-23%)	2.27 (-24%)
WHM05	4.66	3.59	3.47 (-25%)	2.78 (-23%)	3.03 (-35%)	2.11 (-41%)
WHM07	2.11	1.52	1.69 (-20%)	1.48 (-3%)	2.07 (-2%)	1.72 (+14%)

Table 5. Results C2, spectral mean and peak wave periods $T_{m-1,0}$ and T_p (s)

	PHM $T_{m-1,0}$ (s)	PHM T_p (s)	SWS $T_{m-1,0}$ (s)	SWS T_p (s)	SWN $T_{m-1,0}$ (s)	SWN T_p (s)
GRSM1	10.74	14.12	11.47 (+7%)	14.83 (+5%)	10.04 (-6%)	14.16 (+0%)
GRSM2	11.46	14.12	11.91 (+4%)	14.52 (+3%)	10.98 (-4%)	14.16 (+0%)
GRSM3	10.37	9.72	11.13 (+7%)	9.48 (-2%)	8.96 (-14%)	14.16 (+46%)
GRSM4	10.75	17.27	12.28 (+14%)	14.62 (-15%)	8.64 (-20%)	14.16 (-18%)
WHM01	10.62	15.55	13.35 (+26%)	15.28 (-2%)	8.98 (-15%)	14.16 (-9%)
WHM02	11.36	15.55	11.70 (+3%)	17.06 (+10%)	10.89 (-4%)	14.16 (-9%)
WHM03	10.13	15.55	11.66 (+15%)	17.20 (+11%)	8.96 (-12%)	14.16 (-9%)
WHM04	9.88	15.55	10.99 (+11%)	9.57 (-38%)	9.02 (-9%)	14.16 (-9%)
WHM05	10.04	9.14	10.98 (+9%)	7.18 (-21%)	8.43 (-16%)	14.16 (+55%)
WHM07	9.46	9.14	12.17 (+29%)	9.43 (+3%)	10.21 (+8%)	14.16 (+55%)

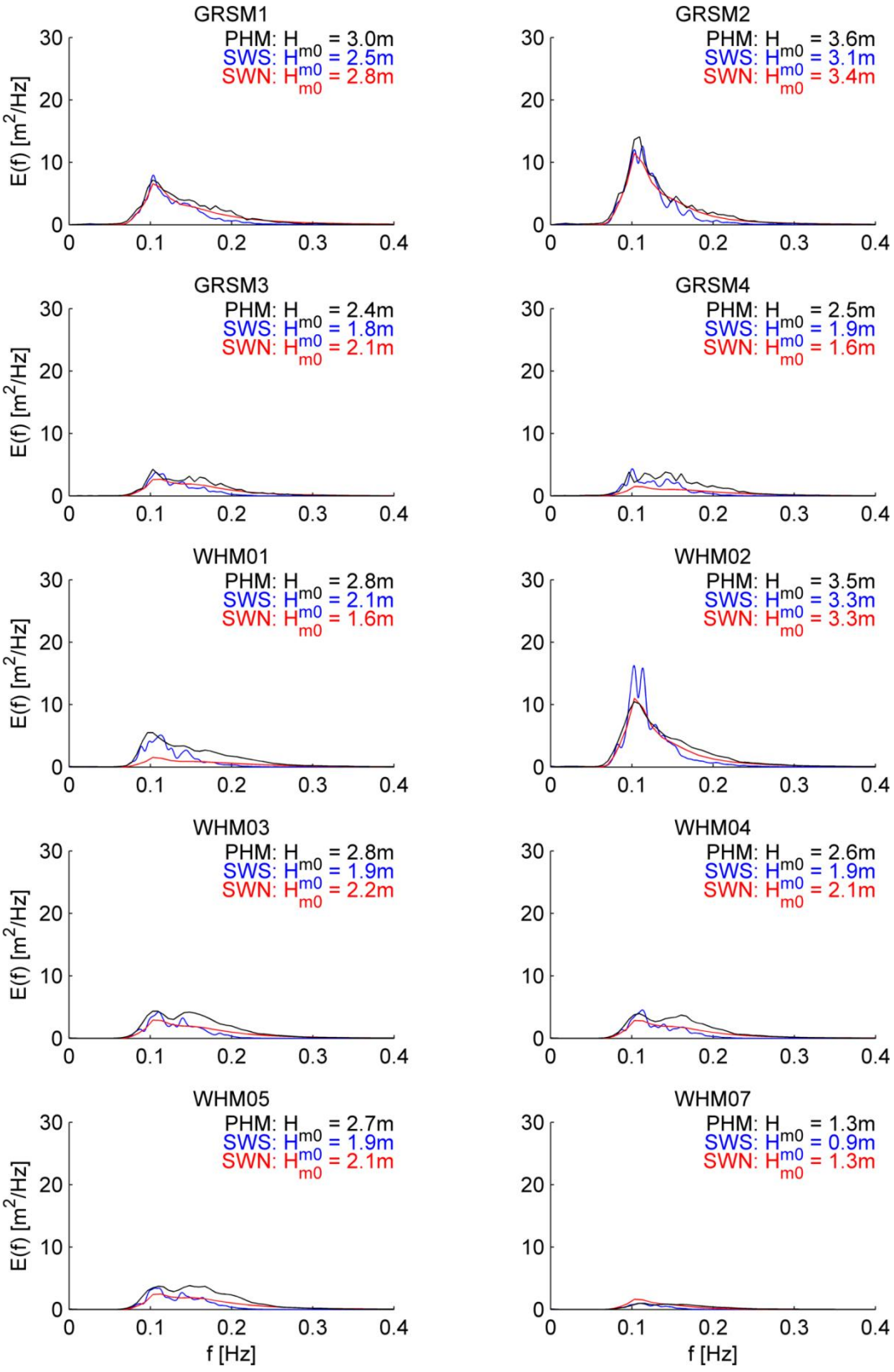

Figure 5. Frequency wave spectra at the WHM and GRSM wave gauges for all models. Black: physical model (PHM), blue: SWASH (SWS), red: SWAN (SWN), scenario C1.

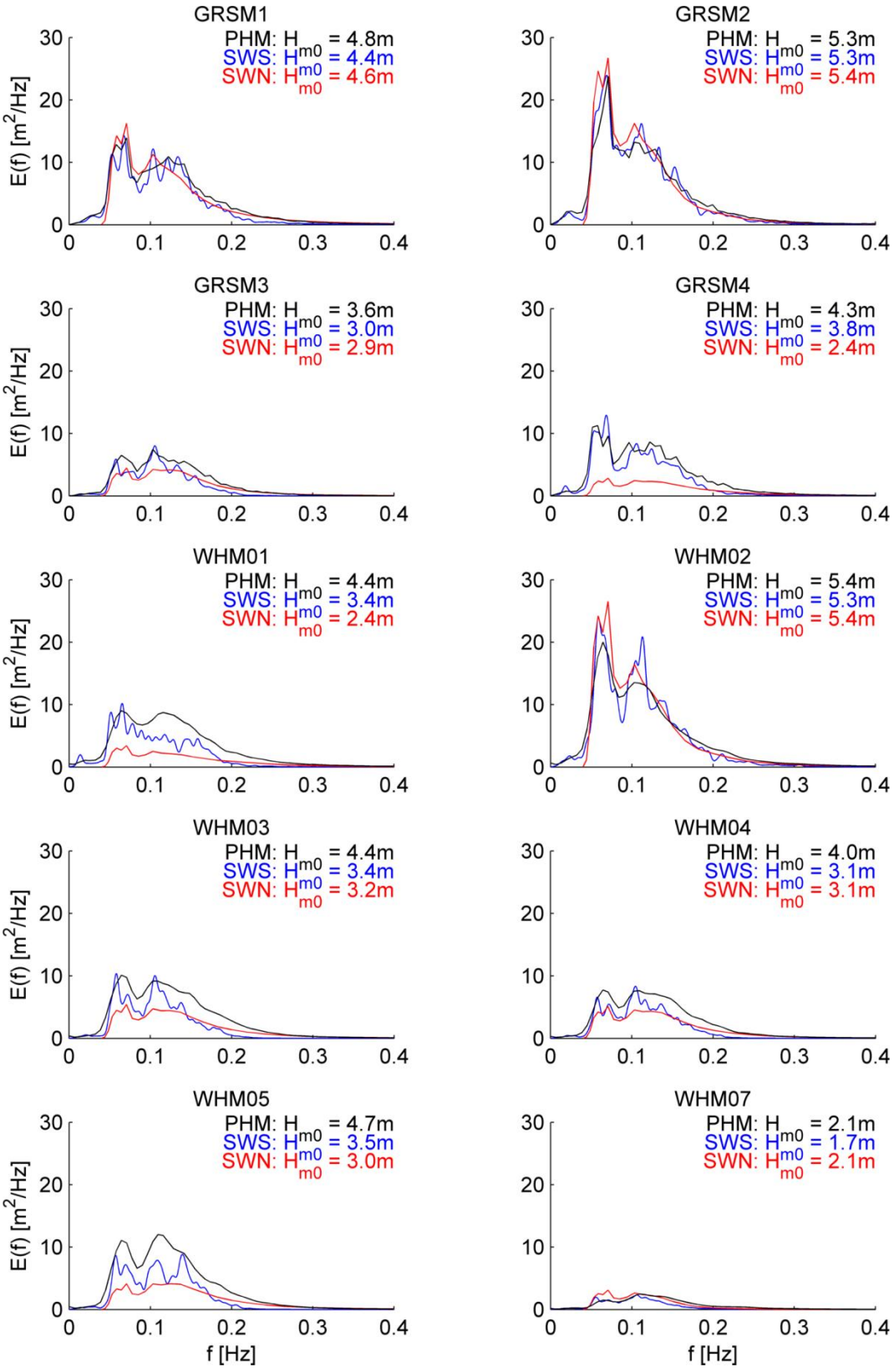

Figure 6. Frequency wave spectra at the WHM and GRSM wave gauges for all models. Black: physical model (PHM), blue: SWASH (SWS), red: SWAN (SWN), scenario C2.

The measured wave parameters and spectra show that:

- The navigation channel significantly affects the (incident) waves, by refraction, diffraction and nonlinear effects, which has a significant impact on the layout and design of the harbor.
- The physical model results clearly show the wave attenuation along the wave-ward side of the channel, by refraction. For scenario C1, this leads to an increase of the significant wave height H_{m0} at GRSM2 (just in front of the breakwater) of 0.6 m (+20%) and 0.5 m (+11%) for scenario C2, as waves start to break (H/d ratio is ~ 0.5) here.
- Inside the navigation channel (GRSM3) H_{m0} decreases to 2.4 m (-22%) and 3.6 m (-26%) for scenarios C1 and C2 respectively. Across the channel – at the lee-ward side (GRSM4) – the significant wave height H_{m0} increases again up to 2.5 m (+6%) and 4.3 m (+21%), compared to the conditions at the channel axis.
- The mean wave period $T_{m-1,0}$ remains relatively stable over the domain, but increases by 6-7% at the wave-ward side (GRSM2), due to the refraction of especially the low wave frequencies, and decreases in the channel by 4-8% (GRSM3), as here the spectrum is dominated by the crossing, higher-frequency waves.

The intercomparison of the measurements with the numerical SWAN and SWASH model results shows that:

- The spectral shape at all locations is very well reproduced by the numerical models (with the exception of the earlier discussed dampened high frequency tail in SWASH). This provides confidence in the adopted method of comparing the model by means of the frequencies ≤ 0.13 Hz.
- SWASH performs very well at the directional wave gauges (GRSM), for both scenarios. The mean error of the significant wave heights $H_{m0;\leq 0.13Hz}$ is -6% and -4% for scenarios C1 and C2 respectively. At the standard resistant type wave gauges (WHM), the mean error of the significant wave heights $H_{m0;\leq 0.13Hz}$ is slightly larger: -6% and -10% for scenarios C1 and C2 respectively, but still the performance is considered good. For both scenarios, WHM05 seems to be an outlier (errors of -23% and -14% respectively) in the physical experiment.
- The mean error in the mean spectral wave period $T_{m-1,0}$ by SWASH is +14% for both scenarios and all locations; a result of the dampened high frequency tail in SWASH.
- SWAN also performs very well at the GRSM1 and GRSM2, for both scenarios, but significantly underestimates the conditions inside and at the lee-side of the channel. The errors in significant wave height $H_{m0;\leq 0.13Hz}$ at GRSM3 are -13% (C1) and -21% (C2), and -36% (C1) and -50% (C2) at GRSM4. Also at WHM01 (also at the lee-ward side of the channel), the mean error in significant wave height $H_{m0;\leq 0.13Hz}$ is -47%.
- The mean error in the mean spectral wave period $T_{m-1,0}$ by SWAN is -7% for both scenarios and all locations; confirming that especially the low frequencies inside and at the lee-ward side of the channel are underestimated by SWAN (the error is significant for scenario C2 – which is dominated by low-frequency waves; -14% at GRSM3 and -20% at GRSM4).
- Also to the peak wave periods are reasonably reproduced by both models. One prominent outlier can be observed at GRSM4, but is the results of a relatively small energy shift between the two distinguished low-frequency peaks (between 0.05-0.07 Hz).

The results confirm that the navigation channel significantly affects the (incident) waves, not only by refraction, but also diffraction and nonlinear effects play a significant role. Simulations with a mild-slope model (Berkhoff, 1972) are carried out to quantify (linear) diffraction effects on the wave reflection and transmission, both below and above the critical wave angle θ_{cr} according to refraction theory. Results are presented as a function of the dimensionless wave period outside the channel $T_0\sqrt{(g/h_1)}$ and the water depth ratio h_2/h_1 outside and inside the navigation channel for two channel widths of 150 m (15 h_1) and 250 m (25 h_1), see Fig. 7. The channel slopes for both widths are 1:5. In Fig. 1 the critical angle θ_{cr} according to refraction theory is presented. In comparison, Fig. 7 presents the critical angle according to the mild-slope equation (MSE). Here, for the angle θ below the MSE critical angle, the transmitted waves are at least 20% in height of the incident wave height. As can be seen, the diffraction effects are most pronounced for long waves, *i.e.* large $T_0\sqrt{(g/h_1)}$. Also, the effects decrease with increasing channel width: since the evanescent waves in the deep part of the channel attenuate, a wider channel means less wave transmission for $\theta > \theta_{cr}$. Figs. 1 & 7 can be used to decide whether refraction theory suffices for a certain channel lay-out and wave conditions.

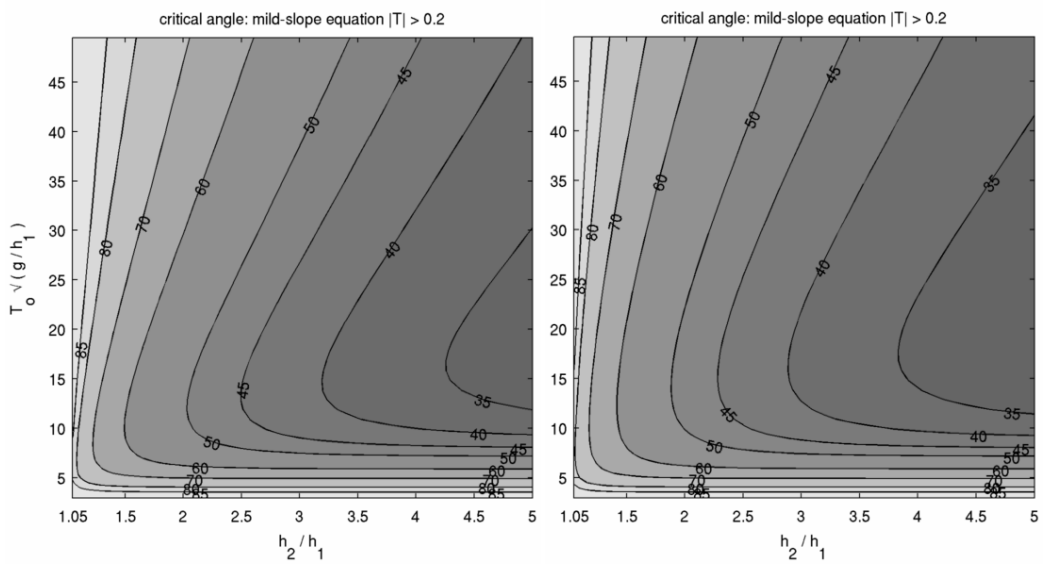

Figure 7. Critical wave angle θ_{cr} based on the mild slope equation as a function of dimensionless wave period outside the channel $T_0\sqrt{(g/h_1)}$ and the water depth ratio h_2/h_1 outside and inside the navigation channel. Left: channel width of 150 m (15 h_1), right: channel width of 250 m (25 h_1).

CONCLUSIONS AND RECOMMENDATIONS

Conclusions and discussion

In this study we have presented results on wave transformation by a navigation channel towards a breakwater-protected harbor entrance, using three types of multi-directional random-wave models: a spectral wave model (SWAN), a phase-resolving model (SWASH) and physical model laboratory tests. The focus is on waves that propagate in a direction relatively small compared with the channel axis direction. Then, for longer waves, a substantial part of the incoming multi-directional wave spectrum travels at angles where waves cannot cross the channel according to refraction theory.

The intercomparison shows that SWAN may significantly underestimate the wave conditions inside and at the lee-side of the channel. SWASH performs better in this respect, and much better for lower storm conditions, showing the importance of incorporating diffraction. At the wave-ward side of the harbor entrance, both numerical models perform well, due to the limiting of the enhanced wave heights by depth-limited wave breaking.

Wave refraction and diffraction are well represented in the spectral wave-energy model SWAN for short-crested, directionally waves. However, for large wave-height gradients (i.e. swell waves in combination with steep channel slopes), SWAN overestimates the reflection of waves – and underestimates wave transmission – by the channel due to the neglect of the effects of wave tunneling by diffraction and evanescent modes. These effects can to be taken into account by setting up a SWASH model (or, with less refinement, by using a phase-resolving mild-slope or Boussinesq-type model) or by performing laboratory tests. Otherwise it may lead to under- or overestimating the wave conditions outside – and wave penetration into – a harbor basin.

Recommendations

An initial assessment of the importance of diffraction on the wave effects caused by the navigation channel can be made using Fig. 7. This evaluation can be made using the relative wave period $T_0\sqrt{(g/h_1)}$, the relative channel depth h_2/h_1 and the incoming wave angle θ. When diffraction effects are important, an appropriate model incorporating this has to be used.

The comparison of SWASH with the physical-model test results shows that SWASH is capable to accurately reproduce the wave conditions in combined refraction-diffraction conditions – for the low-frequency part of the wave spectrum it can resolve on a certain computational grid. The high-frequency part of the spectrum can be estimated using SWAN (since the short waves are always capable to cross the channel). Combining the low-frequency part of SWASH and high-frequency part by SWAN gives the total wave spectrum (and resulting significant wave height). Alternatively, the high-frequency part for the spectrum of the SWASH computations can be estimated by use of a power-law high frequency tail of the spectrum, *e.g.* proportional to f^4, the fourth power of the frequency.

REFERENCES

Berkhoff, J.C.W., 1972: Computation of combined refraction–diffraction, Proc. 13th Int. Conf. Coastal Engineering, Vancouver, 471–490.

Booij, N., 1983: A note on the accuracy of the mild-slope equation, Coastal Engineering, **7**(3) 191–203.

Booij, N., R.C. Ris, and L.H. Holthuijsen, 1999: A third-generation wave model for coastal regions, Part I, Model description and validation, J. Geophys. Res., **104**(C4), 7649–7666.

Chamberlain, P.G., and D. Porter, 1995: The modified mild-slope equation, J. Fluid Mechanics, **291**, 393−407.

D'Angremond, K., J.W. van der Meer and R.J. de Jong, 1996: Wave transmission at low-crested structures, Proc. 25th Int. Conf. Coastal Eng., Orlando, FL, USA, 2418–2427

Dusseljee, D.W., C. Kuiper, and G. Klopman, 2012: Wave modelling in navigation channels, Proc. 4th Int. Conf. of the Application of Physical Modelling to Port and Coastal Protection – Coastlab12, Ghent, Belgium, 465–474.

Guzmán Mardones, C.A., 2011: Impact of access channel geometry on wave penetration in harbours, MSc Thesis, Delft University of Technology.

Holthuijsen, L. H., Herman, A., and N. Booij, 2003: Phase-decoupled refraction–diffraction for spectral wave models. Coastal Engineering, **49**(4), 291–305.

Hurdle, D.P., J.K. Kostense, and P. van den Bosch, 1989: Mild-slope model for the behaviour in and around harbours and coastal structures in areas of variable depth and flow conditions. Proc. 2nd Int. Symp. Water Modelling and Measurement, 307–324.

Kirby, J.T., 2003: Boussinesq models and applications to nearshore wave propagation, surfzone processes and wave-induced currents. Advances in coastal modelling, **67,** 1–41.

Kirby, J.T., and R.A. Dalrymple, 1983: Propagation of oblique incident water waves over a trench, J. Fluid Mechanics, **133**, 47–63.

Kuik, A.J., G.Ph. van Vledder, 1988: A method for the Routine Analysis of Pitch-and-Roll Buoy Wave Data. Journal of Phys. Oceanogr., 18, 1020-1034.

Li, Y.S., S.-X. Liu, O.W.H. Wai, and Y.-X. Yu, 2000: Wave concentration by a navigation channel, Applied Ocean Res., **22**(4) 199–213.

Ma, Q., 2010: Advances in numerical simulation of nonlinear water waves, World Scientific, Advances in coastal and ocean engineering, **11.**

Magne, R., K.A., Belibassakis, T.H.C. Herbers, F. Ardhuin, W.C. O'Reilly, and V. Rey, 2007: Evolution of surface gravity waves over a submarine canyon. Journal of Geophys. Res., **112**, C01002.

Misra, S. K., A.M. Driscoll, J.T. Kirby, A. Cornett, P. Lomonaco, O. Sayao, and M. Yavary, 2008: Surface gravity wave interactions with deep-draft navigation channels – physical and numerical modelling case studies, Proc. 31st Int. Conf. Coastal Engineering, Hamburg, August 31 – September 5, 2786–2798.

Porter, D., 2003: The mild-slope equations, J. Fluid Mechanics **494,** 51–63.

Van Vledder, G. Ph., and M. Zijlema, 2014: Non-hydrostatic wave modelling in partly sheltered areas. Proc. 34th Int. Conf. on Coastal Eng., Seoul, South Korea.

Zijlema, M., G. Stelling, and P. Smit, 2011, SWASH: An operational public domain code for simulating wave fields and rapidly varied flows in coastal waters, Coastal Engineering **58**(10), 992–1012.

Zwamborn, J.A., and G. Grieve, 1974, Wave attenuation and concentration associated with harbours approach channels, Proc. 14th Int. Conf. Coastal Eng., Copenhagen, June 24–28, Denmark, 2068–2085.